Combustion and Flame 244 (2022) 112233

Contents lists available at ScienceDirect

Combustion and Flame

journal homepage: www.elsevier.com/locate/combustflame

Release characteristics of potassium and sodium during pellet combustion of typical MSW fractions using the FES method

Junjie He[a], Jiayu Li[a], Qunxing Huang[a,b,*], Jianhua Yan[a]

[a] State Key Laboratory of Clean Energy Utilization, Institute for Thermal Power Engineering, Zhejiang University, Hangzhou 310027, China
[b] Alibaba-Zhejiang University Joint Research Institute of Frontier Technologies, China

ARTICLE INFO

Article history:
Received 24 September 2021
Revised 14 May 2022
Accepted 30 May 2022
Available online 14 June 2022

Keywords:
Municipal solid waste (MSW)
Flame emission spectroscopy (FES)
Alkalis
Combustion

ABSTRACT

The temporal release characteristics of sodium and potassium (Na and K) during the pellet combustion of municipal solid waste (MSW) were comparatively studied using calibrated flame emission spectroscopy (FES). A lab-scale setup with a Hencken burner was used to create a stable high-temperature environment for pellet ignition and combustion. The results revealed a three-stage combustion process (devolatilization, char, and ash stages) for most waste fractions, whereas a one-peak release distribution was observed for plastics. In contrast, biomass-based products and kitchen waste were characterized by dual-maxima release shapes. In general, the release concentrations of both Na and K were the highest in the char and ash stages because of the higher pellet surface temperature than that in the devolatilization stage. Although the variation in pellet mass changed significantly during devolatilization, less than 10% of alkali contents were released. Compared to the combustion characteristics, the waste compositions were considered a critical factor. The peak release concentrations increased almost linearly with the initial alkali concentrations during char oxidation. In addition, paper and wood waste were found to be the potential sources for the release of Na and K, respectively, second only to kitchen waste. Finally, the possible transformation processes of alkalis during waste combustion were discussed.

1. Introduction

The disposal of municipal solid waste (MSW) has attracted increasing attention due to China's rapid urbanization and industrialization [1]. Currently, incineration is widely used to realize harmless disposal, energy recovery, and volume reduction of MSW [2]. However, untreated MSW which varies largely in physical and chemical composition is generally rich in alkali and alkaline earth metals [3]. During combustion, these volatile elements especially potassium (K) and sodium (Na) are prone to vaporize into the gas phase and form sticky deposits on the heat exchange surfaces [4], which eventually results in significant problems of slagging, fouling, and corrosion. Therefore, knowledge of the release characteristics of typical alkali elements during combustion is essential to guide combustion optimization and the stable operation of the boiler system.

Over the last few decades, studies on alkali detection have evolved from offline to online measurements. This is because the traditional offline techniques [5,6], such as X-ray diffraction (XRD), energy dispersive X-ray spectroscopy (EDX), and X-ray fluorescence spectrometer (XRF), can identify alkali species and quantitatively obtain the total amounts of alkali metals in fuel and ash, but cannot provide time-resolved information on the alkalis released during combustion. Therefore, non-invasive, real-time optical diagnostic techniques are promising for studying the release behaviors of alkalis in laboratories. Laser-Induced breakdown spectroscopy (LIBS), for instance, has been employed to perform quantitative point measurements of Na and K released during coal and pinewood combustion by Hsu et al. [7]. Liu et al. [8,9] proposed a multiple-point LIBS method to measure alkali concentrations in the gas phase. Based on the potassium release characteristics of burning poplar and corn straw, possible reaction mechanisms were proposed [9] to describe the transformation of elemental and atomic potassium during combustion. Although multiple laser-based optical methods are commonly used to measure flame gas/particle concentration, flame temperature, and flue gas velocity [10,11], they are rarely applied to industrial incinerators due to their harsh environment.

Flame emission spectroscopy (FES), as a promising *in-situ* diagnostic technique based on the chemiluminescence phenomenon, can retrieve important combustion information through the received self-radiative signal of the flames and feature a much simpler device and lower cost for laboratory experiments and even on-site applications [12]. This technique is primarily applied in com-

* Corresponding author at: State Key Laboratory of Clean Energy Utilization, Institute for Thermal Power Engineering, Zhejiang University, Hangzhou 310027, China.
E-mail address: hqx@zju.edu.cn (Q. Huang).

https://doi.org/10.1016/j.combustflame.2022.112233
0010-2180/

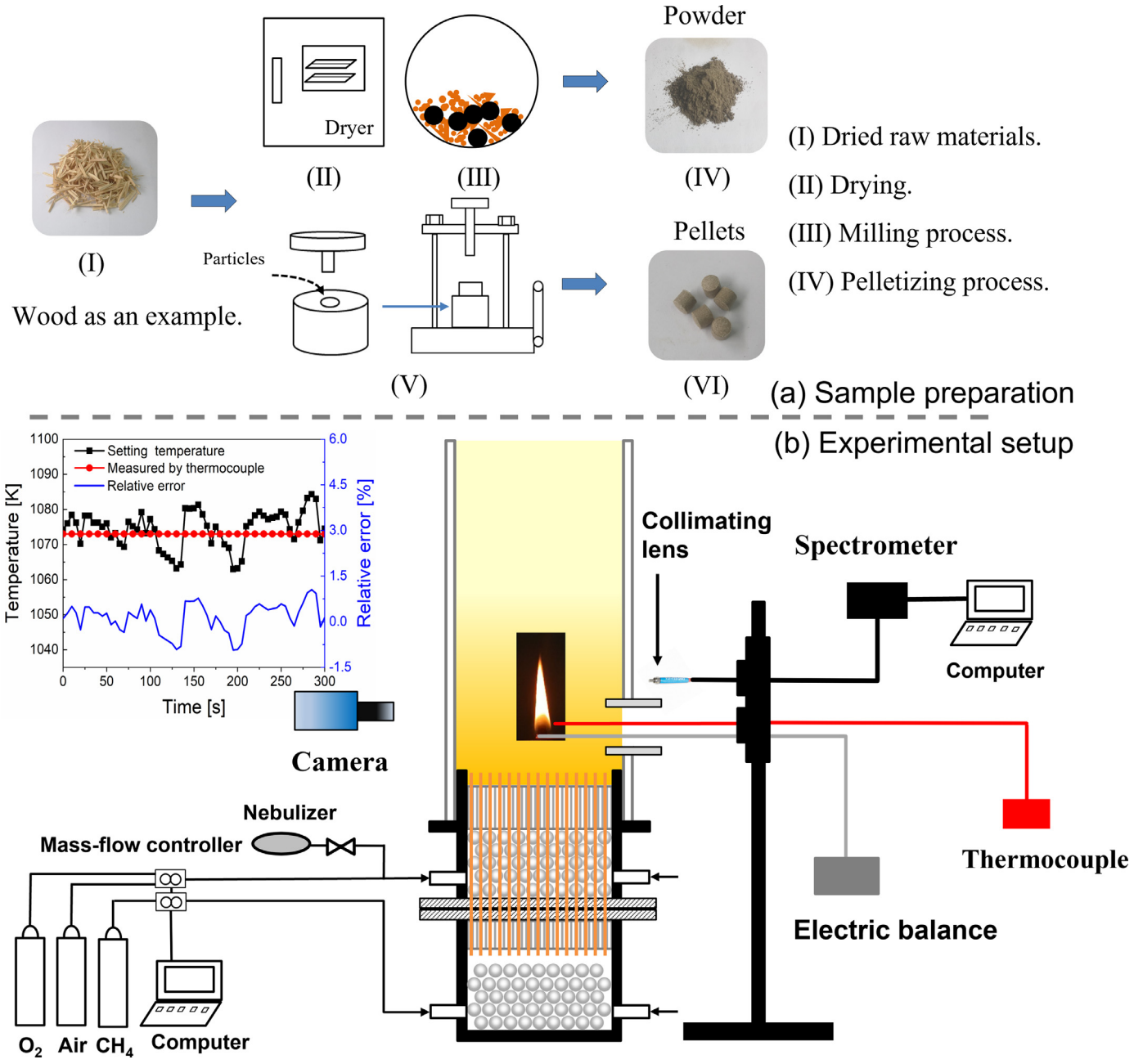

Fig. 1. Schematic diagram of *in situ* fuel pelletizing process (a) and combustion and FES experimental setup (b).

bustion diagnostics for detecting OH*, CH* and C2* flame radicals [13,14] and is also used to make real-time measurements of alkalis in flames. Paulauskas et al. [15] used an inductively coupled plasma mass spectrometer (ICP-MS) to verify the FES data. The results revealed that the FES technique was capable of online monitoring the release of alkali species from biomass burning. Mason et al. [16] measured the K release patterns from burning biomass pellets and later established a potassium release model to predict the temporal release of gaseous potassium [17]. He et al. [18] used the FES method to further study the effects of biomass composition and moisture content on the K release patterns from the combustion of camphorwood and rice husks. The results showed that the change in moisture content affected the ratio of K released from the biomass with a low share of volatiles. Note that the above investigations were conducted simply by assuming that the combustion temperature was constant, but the temperature of the flames actually changes continuously. Thus, Li et al. [19,20] proposed a calibration method between alkali concentrations, temperature, and spectral line intensity and further used the improved FES method to measure the temporal release profiles of Na and K from burning biomass and coal, respectively. They discovered that the high spectral intensity of Na and K did not result in high release concentrations in the flame, where the temperature acted as a significant factor.

Despite these efforts, most other similar investigations are still based on the combustion of biomass and coal [21,22]. However, minimal information is available on the release properties of alkalis during the combustion of municipal solid waste. He et al. [23] recently conducted *in situ* FES measurements of alkali metals in two MSW incinerators. The results indicated that the released gaseous K and Na concentrations were correlated with the volatile and alkaline contents of the waste, combustion temperature, and

Table 1
The main properties of the test samples in this work [24].

Materials	Proximate analysis(wt.% on air dry basis)				Ultimate analysis(wt.% on air dry basis)					Content(mg/kg)	
	M	A	V	FC	C	H	O	N	S	Na	K
Wood	1.8	0.7	80.8	17.0	49.5	6.4	41.4	0.06	0.21	1219	4890
Bamboo	1.4	0.9	79.6	18.1	49.8	6.3	41.3	0.10	0.17	1028	5854
Leaves	1.7	11.5	68.2	18.6	45.1	5.5	34.5	1.44	0.15	723	12,374
Cardboard	1.7	10.8	76.4	11.1	41.3	5.2	40.6	0.19	0.15	1987	3014
Tissue paper	1.8	0.5	87.6	10.1	44.2	6.4	46.7	0.02	0.49	3987	2019
Office paper	1.7	11.4	75.6	11.3	37.7	4.7	44.4	0.07	0.10	2215	2458
Cotton fabric	5.2	0.5	85.6	8.7	43.2	6.1	44.1	0.27	0.78	785	1583
Nonwoven	0.9	5.1	93.7	0.3	77.3	14	2.4	0.02	0.22	1122	2236
PE bag	0.5	3.0	96.0	0.5	79.1	17	2.2	0.01	0.71	1213	619
Wood waste	1.7	4.4	77.1	16.8	44.1	6.1	41.8	0.15	0.16	2089	10,588
Paper	1.7	5.6	81.9	10.8	41.1	5.4	43.9	0.10	0.20	2567	2334
Kitchen waste	4.5	10.2	64.8	20.5	39.2	6.8	45.2	0.45	0.09	13,604	21,235
Textiles	0.7	3.2	89.9	6.2	45.6	3.5	40.1	1.20	0.85	4523	3612
Plastic	1.6	2.1	91.5	4.8	59.2	6.0	33.5	0.20	0.56	1166	210
MSW mixture	3.5	8.1	71.7	16.6	42.6	6.4	43.1	0.39	0.20	7254	9539

M: moisture, A: ash matter, V: volatile matter, FC: fixed carbon.

primary air in the furnace, despite the limited deeper elaboration on the phenomenon. The regions and seasons could significantly affect the physical composition of MSW [1], thereby leading to significant variations in Na and K contents. However, little experimental or computational research has been conducted on the release characteristics during the combustion of specific municipal solid waste fractions to the best of our knowledge.

The present study aims to better understand the release behaviors of sodium and potassium during the combustion of different municipal solid waste fractions. The experiments were performed in a lab-scale combustion setup, creating a stale and high-temperature environment for waste-pellet combustion. The *in-situ* FES technique was employed to obtain the time-resolved release profiles of atomic alkali metals during combustion. In addition, the surface temperature and mass of the pellets were simultaneously recorded. Based on these combined measurement data, the release characteristics across the waste fractions and possible transformation routes of alkalis are comparatively discussed.

2. Materials and methods

2.1. Materials preparation

Given the complexity of municipal solid waste in physical and chemical compositions, a total of 15 common single/mixed waste fractions were selected as experimental fuel samples [25], which were all selected from Hangzhou, Zhejiang Province, China. Specifically, the nine single fractions mainly included wood waste: wood chopsticks, bamboo chopsticks, leaves, paper (i.e., cardboard, tissue paper, and office paper), and plastic-containing materials (cotton fabric, nonwoven fabric, and PE bag). The six typical mixed fractions were kitchen waste, wood waste, paper, textiles, plastics, and MSW mixtures, all sampled by hand from waste piles. The main properties of the samples are listed in Table 1. The mass of the oxygen fraction was calculated according to the mass balance, and the initial sodium and potassium concentrations in the solid wastes were determined via inductively coupled plasma atomic emission spectroscopy (ICP-AES) [9]. As shown in Table 1, plastic (textiles) fractions had a high share of volatile matter, while biomass materials, such as paper and wood waste, had a high share of fixed carbon. The initial contents of Na and K also varied among the waste samples, with kitchen waste possessing the highest proportion of alkalis.

Before the experiment, the materials were made into pellets for subsequent combustion measurements following the on-site pelletizing process, as shown in Fig. 1a. First, all the materials were dried in an oven at 105 °C overnight. Then, they were crushed, milled into a fine powder, and sieved to obtain 250 μm particles. Subsequently, approximately 120 mg ($\pm$1 mg) of the uniform powders was manually pressed into spherical pellets with a diameter of 6 mm for consistency.

2.2. Experimental setup

The setup of the laboratory-scale FES measurement system is shown in Fig. 1b. A Hencken burner was used to provide a stable high-temperature environment for the ignition and combustion of pellets. The complete details regarding the design principle of the burner can be found in Ref. [26]. For the burner, methane was the fuel gas with a constant flow rate of 0.6 L/min, while the air was the oxidant with a constant flow rate of 8 L/min. A hyaline quartz tube drilled with a feeding hole was placed above the burner to reduce the heat loss during the experiment. The waste pellet was suspended on two ceramic rods (diameter 0.8 mm) and burned in the chamber in each trial. The temperature at the pellet height was set to approximately 1073 K, which is typical for incineration applications. The stability of the temperature was tested beforehand, as shown in Fig. 1b, where the maximum error was no more than 1.5%. Because the plastic-containing fractions melted when combusted, Pt wires were wrapped around the ceramic rods in order to avoid the falling drop of the melted plastics during combustion.

As shown in Fig. 1b, an AvaSpec-ULS2048L-USB2 spectrometer with a response wavelength range of 200–1100 nm was used to capture FES signals 10 mm above the burning pellet *in-situ*. The combustion images were recorded using a digital camera at 30 frames/s. In contrast, the variations in pellet mass and surface-pellet temperature during combustion were obtained using an electric balance and thermocouple, respectively. The ceramic rods were cleaned prior to the next experiment to eliminate interference from the residue on the spectral line intensity of the alkalis. For the FES measurements, each trial was performed at least three times to ensure reliable repeatability of the experiments. The standard deviation was calculated from parallel experiments and was shown in the figure.

2.3. Calibration of FES system

Since the outputs of the spectrometer were just the relatively radiative intensities (Counts) along the wavelength, a necessary calibration using a blackbody furnace (FuYuan, HFY-203B) was carried out to obtain the absolute spectral radiation profiles. Figure 2a shows the calibration results of the spectrometer, in

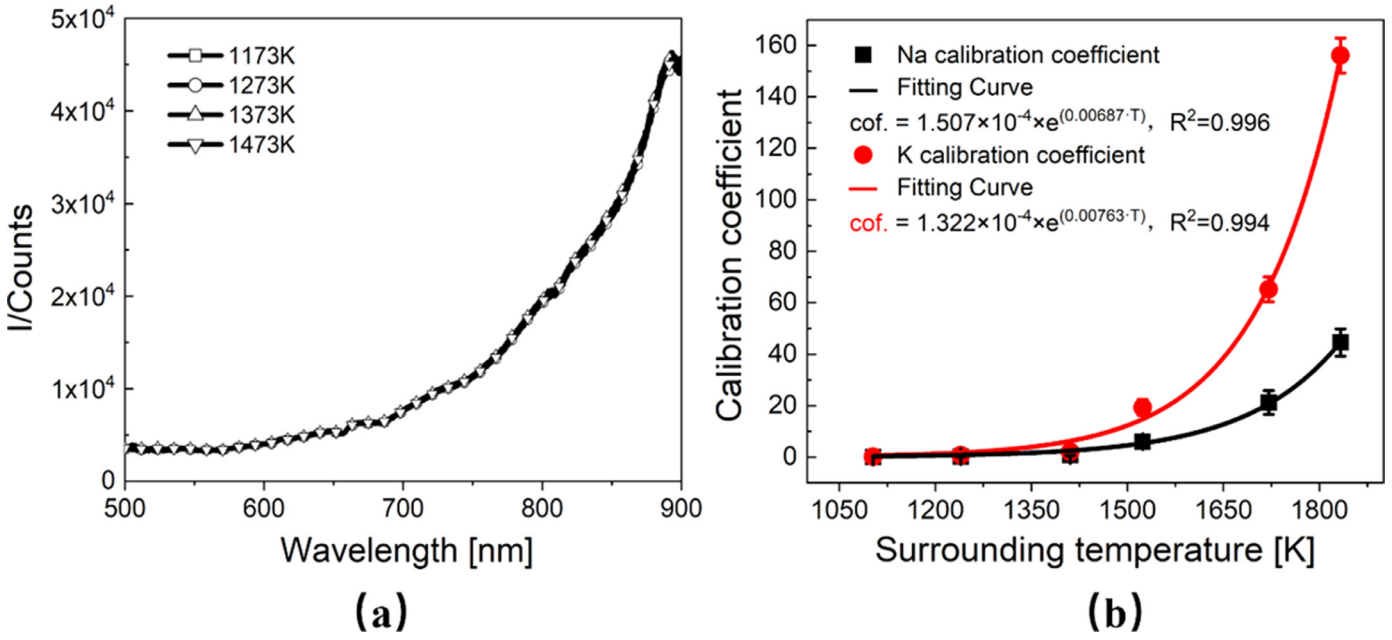

Fig. 2. Calibration results for the spectrometer (a) and the atom concentrations of alkali metals (b).

which the coefficient curves hardly changed with the temperature of the black furnace (1173–1473 K). Generally, the thermal radiation of the flame $I(\lambda, T)$ serves as a function of the wavelength (λ) and temperature (T) which can be described by Planck's law:

$$I(\lambda, T) = \varepsilon(\lambda) I_b(\lambda, T) = \varepsilon(\lambda) \frac{C_1 \lambda^{-5}}{\pi \times (e^{C_2/(\lambda T)} - 1)} \quad (1)$$

Where $I_b(\lambda, T)$ is the blackbody radiation intensity (W/m^3), $\varepsilon(\lambda)$ is the flame emissivity, C_1 is the Planck's first radiation constant (3.7419×10^{-16} W•m^2), C_2 is the Planck's second radiation constant (1.4388×10^{-2} m•K).

The radiation intensities (I_m) are the sum of the spontaneous thermal radiation intensity (I_c) and the characteristic line intensities of sodium and potassium ($I_{Na} + I_K$) [27]. As reported, alkali species released into the flame are thermally excited such that the spectral intensity is proportional to the concentration of volatilized alkalis in the gas phase [7]. For quantitative measurements of alkali concentrations in the flame, the FES system under study also needs calibration, the details of which can be found in Ref. [20].

In the calibration experiment, the prepared sodium chloride (NaCl) and potassium chloride (KCl) solutions with known concentrations ranging from 100 to 1800 ppm were seeded into a flat flame through a nebulizer. The average seeding rate of the solutions was approximately 0.11 g/min. Assuming that the alkali salts were uniformly distributed in the flat flames produced by the burner, the concentrations of gaseous K and Na in flame C (mg/m^3) can be expressed as follows:

$$C = \frac{V_s \times C_s \times R \times T_r}{V_m \times p \times (v_g + v_a)} \quad (2)$$

where C_s is the concentration of alkali salt in the solution (mol/L) while V_s is the consumption rate of alkali salt (L/min), R is ideal gas constant (8.31 Pa•m^3/(mol•K)), T_r is room temperature, p is pressure (pa), v_g and v_a are flow rates of methane and air, respectively (mol/min), and V_m is the gas molar volume (mol/min). Note that the solution fog would inevitably disturb the stability of the flat flames produced at the start of the experiment; thus, spectral data for the calibration were recorded after the system reached equilibrium.

The FES calibration results for cases with different Na and K concentrations are presented in Fig. S1. This indicated that the concentrations and FES intensity exhibited a non-linear relationship due to the self-absorption effect, especially at high concentrations. After the correct process of self-absorption by the Beer-Lambert law, a linear relationship between the FES intensity and the concentrations of volatilized K and Na was obtained. Thereafter, the calibration experiments were performed in parallel at six typical combustion temperatures from 1050 to 1850 K to establish a quantitative relationship between the calibration coefficient and temperature (T). The coefficients of determination (R^2) were at least 95% and the measurement uncertainty of the FES system was mainly due to calibration uncertainty and background noise. As shown in Fig. 2b, the calibration coefficient (α) increased exponentially with the corresponding combustion temperature, consistent with the findings reported by Li and Yan [20]. For the present upset, the observed mathematical relationship can be written as:

$$C_{FES,Na} = \frac{I_{FES,Na}}{1507 \times e^{0.00687 \cdot T}} \quad (3)$$

$$C_{FES,K} = \frac{I_{FES,K}}{1322 \times e^{0.00763 \cdot T}} \quad (4)$$

Where $I_{FES,Na}$ and $I_{FES,K}$ are, respectively the absolute radiation intensity of sodium and potassium, T is the temperature of the measuring point, $C_{FES,K}$ and $C_{FES,Na}$ are the concentrations of alkali metals in the gas phase.

3. Results and discussions

3.1. Release quantification by FES

In this section, the quantitative release profiles of alkali metals during the combustion of wood (poplar), illustrated as an example, are measured using FES. Figure 3a shows a typical relative and calibrated flame emission spectra from volatile combustion. As noted in Section 2.3, spectral curves typically consist of two parts of the continuous radiation spectrum and two characteristic alkali line spectra (Na and K). The continuous radiation spectra were used to calculate the temperature (T) based on a multi-

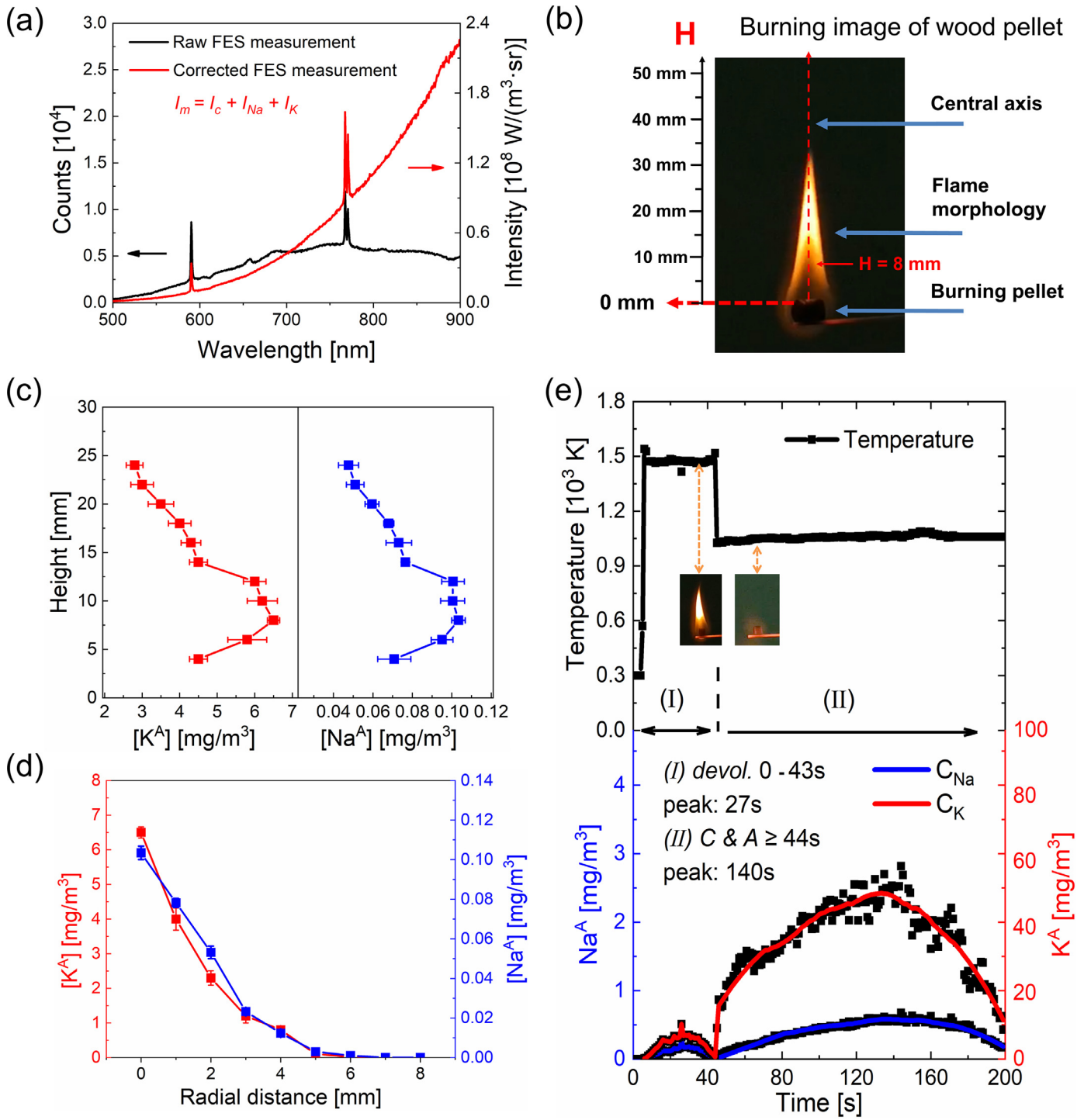

Fig. 3. Release characteristics of sodium and potassium from burning wood: Typical flame emission spectra during combustion (a), combustion image of the wood pellet (b), distributions of alkali concentration axially and radially above the pellet (c,d), and the alkali release history measured by FES (e).

wavelength temperature measuring algorithm [28], where a non-gray emissivity model with a fourth-order polynomial function was determined. Subsequently, $C_{FES,\,K}$ and $C_{FES,\,Na}$ were both solved according to Eqs. (3) and (4), respectively.

A typical image of the volatile flame produced from burning individual wood pellets is shown in Fig. 3b, and additional combustion images for other samples are provided in Fig. S1. This revealed that combustion behaviors underwent three well-differentiated stages: devolatilization, char oxidation, and ash stages, independent of waste type [8,9,18–21]. Herein, the disappearance of visible flames could be considered an indicator of the end of the devolatilization stage, after which the slower, smolder char oxidation stage starts. In the early stages, the combustion performance was a combination of homogeneous and heterogeneous ignition mechanisms [29]. Compared to typical biomass-based products, plastics and fabrics exhibited stronger combustion reactions with relatively higher heights and sizes of volatile flames, as shown in Fig. S1. It has been reported elsewhere that plastic fractions in MSW can improve incineration efficiency and increase the thermal output of the boiler system [30].

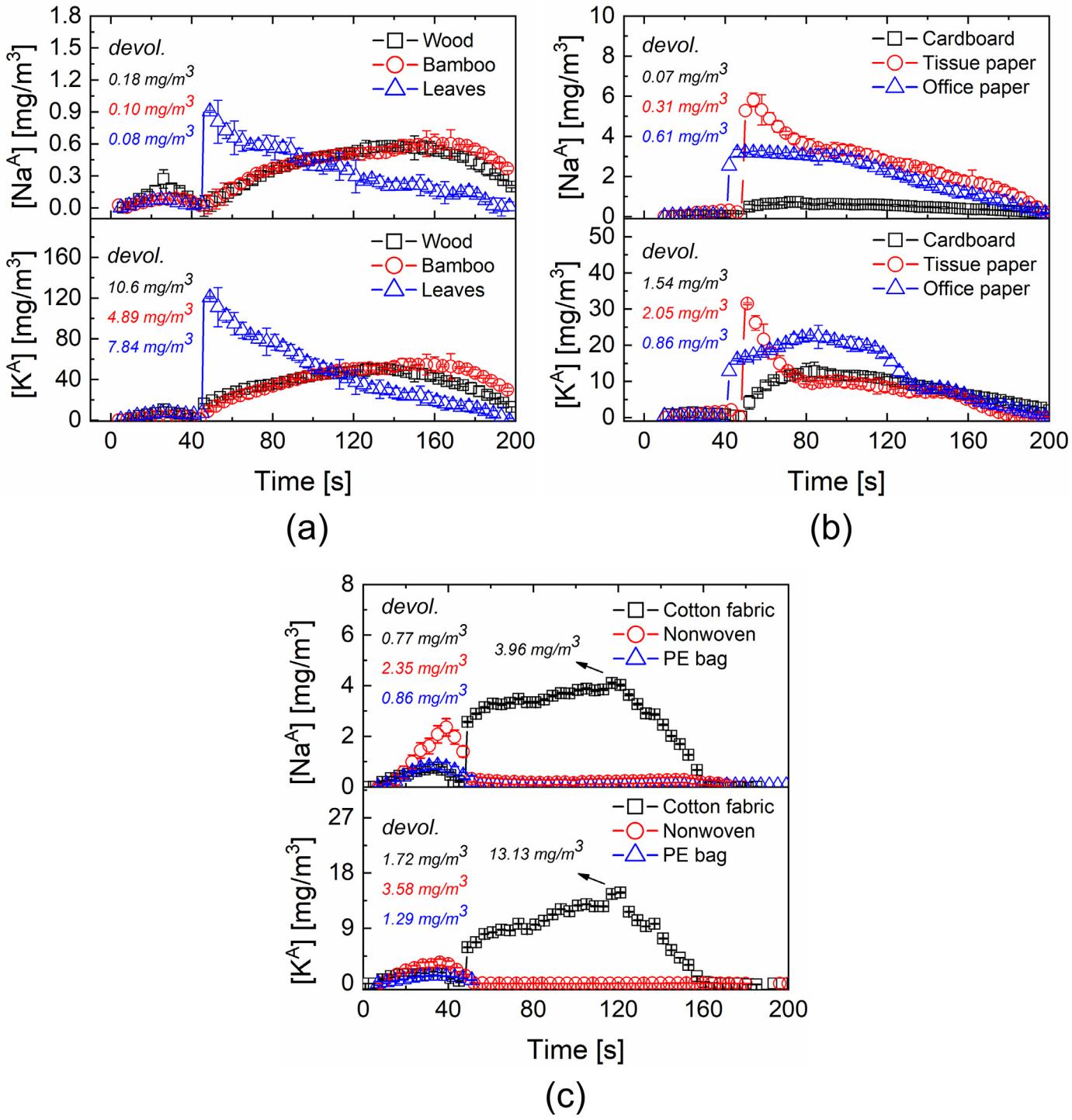

Fig. 4. Temporal release profiles of Na and K ([Na^A] and [K^A]) for single MSW components: fractions of wood waste (a), paper (b), and plastic-containing materials (c).

The distribution of K and Na concentrations along with the axial and radial distances above the 6-mm pellet at approximately 15 s after ignition are plotted in Fig. 3c and d. Overall, the trends in the release concentration, as a function of the axial and radial distances, were similar for both Na and K. Specifically, as the distance from the pellet centerline increased, the concentration gradually increased, and the highest-concentration region appeared at a height of approximately 8 mm, after which the decay began. The diffusion and chemical reactions between the volatiles and air could account for the phenomenon, which was also observed during the early combustion of corn straw and coal [9,31]. In contrast, the concentrations decreased monotonically to zero with an increase in radial distance. It should be mentioned that using the FES technique, only the concentrations of Na and K atoms instead of specific alkali species along the sightline direction were detected in the present work.

Figure 3e shows the FES measurements of the temporal release concentrations of alkali metals performed 10 mm above the wood pellets. As can be seen, there are two maxima in the release profiles, which strongly resemble the experimental results for woody biomass [16]. Precisely, it was observed from the K release profiles that the first minor release peak occurred in the late

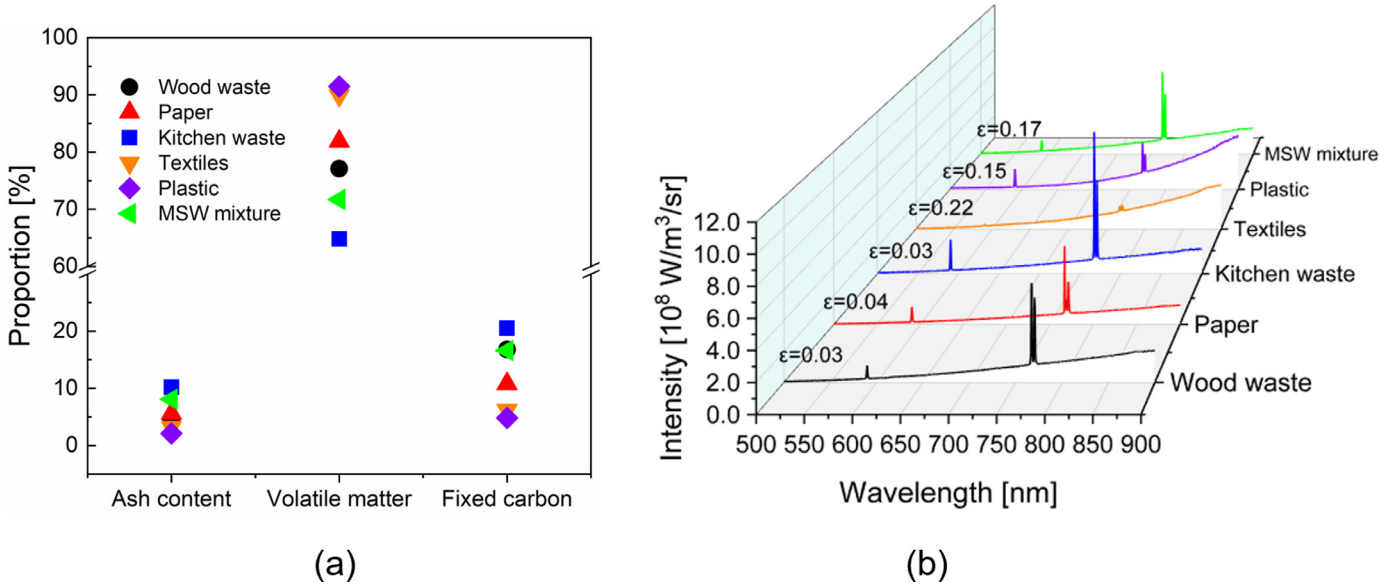

Fig. 5. The properties of the mixed waste (a); Typical emission spectrum of volatile flame for the mixed waste (b).

devolatilization stage (*devol.*) with a maximum concentration of around 9.6 mg/m^3. In comparison, the second one took place in the char and ash stage (C&A) with a much larger peak release concentration of 54.4 mg/m^3, followed by a decay process asymptotically to the baseline. The deviation in K concentrations compared with the results obtained using LIBS [32] may be attributed to the larger pellet quality used in this work, which exhibited an elongated devolatilization duration time and higher release concentrations. The black dotted line readily identified the three stages, which also reflected the changes in the temperature of the measuring point. The results showed that the flame temperature rapidly increased up to 1500 K due to the thermal radiation from burning volatiles and remained steady. After the volatiles were completely combusted, the temperature returned to the gas temperature or slightly lower.

3.2. Release characteristics of single fractions

Figure 4 shows the variations in atomic Na and K concentrations measured over time. The results showed that the temporal release profiles of the selected single biomass-based fractions (paper and wood waste species) exhibited dual-peak shapes, similar to what has been observed in a previous work [7]. In general, the end of the first peak was identified as the devolatilization stage, after which the char and ash stages occurred successively.

As shown in Fig. 4a, the released concentrations of K were higher than those of Na. It is because potassium is essential for the photosynthesis and growth of plants, thereby existing in high proportions in biomass. Moreover, herbaceous crops and straw have higher potassium of 0.2–1% or more than the woody biomass (0.1%). Therefore, the peak release concentration of K from the leaves reached a maximum of 128 mg/m^3 during the char oxidation stage, which was more than twice than that of wood (51 mg/m^3) and bamboo (54 mg/m^3). In a similar study by Liu and Wang [33], the peak K concentration from burning corn straw was more than three times that from burning woody poplar. Another study [34] also found that thermochemical processes in herbaceous biomass materials with high amounts of cellulose were likely to occur at a relatively low reaction temperature compared to woody biomass, which could contribute to the earlier release of potassium. Therefore, the second release peak for leaves was very close to the devolatilization stage, followed by a long monotonic decay. In contrast, wood and bamboo featured a release peak in the late char oxidation stage. In addition, the temporal release profiles of both Na and K from wood and bamboo were similar, probably because of their similar chemical compositions and structures (Table 1).

In addition to wood waste, paper products constitute a large proportion of the biogenic fraction of MSW. From Fig. 4b, the three kinds of papers showed relatively lower K release concentrations but much higher Na release concentrations than the results of wood waste in the devolatilization and char stages. For example, taking tissue paper, the peak concentrations of Na in the gas phase were measured to be 0.31 mg/m^3 and 6.22 mg/m^3 in the stages of devolatilization and char oxidation, respectively. In contrast, the maximum Na release concentration attained no more than 1 mg/m^3 for the wood, bamboo, and leaves. It is also interesting to note that the release mode of tissue paper was closer to that of leaves while the other two were much closer to that of woody biomass. In the case of the PE bag and nonwoven fabric in Fig. 4c, however, only one initial peak of the alkali concentration was characterized in the devolatilization stage because most of the pellet mass was consumed during the overlap combustion of volatiles and char. As expected, cotton fabric made of cellulosic materials showed release characteristics similar to biomass-based products.

In this section, the alkali release characteristics from typical single wastes were analyzed, and the results really revealed significant effect of the waste type on the release performance. In actual MSW incineration, the combustion routes for different components are stirred together, except in extreme cases with only one dominant component. Hence, we further explored the release characteristics of sodium and potassium during the combustion of several mixed wastes in detail in the next section.

3.3. Release characteristics of mixed fractions

3.3.1. Spectral characteristics of volatile flames

Figure 5 showcases the typical emission spectrum during the volatile combustion for six types of mixed waste fractions. As can be seen, plastic-containing species including plastics and textiles clearly showed a relatively larger radiation intensity than the biomass-based products. It implied that the FES signals were associated with the portion of volatile matter in the sample, as shown in Fig. 5a. In essence, the continuous spectrum originated

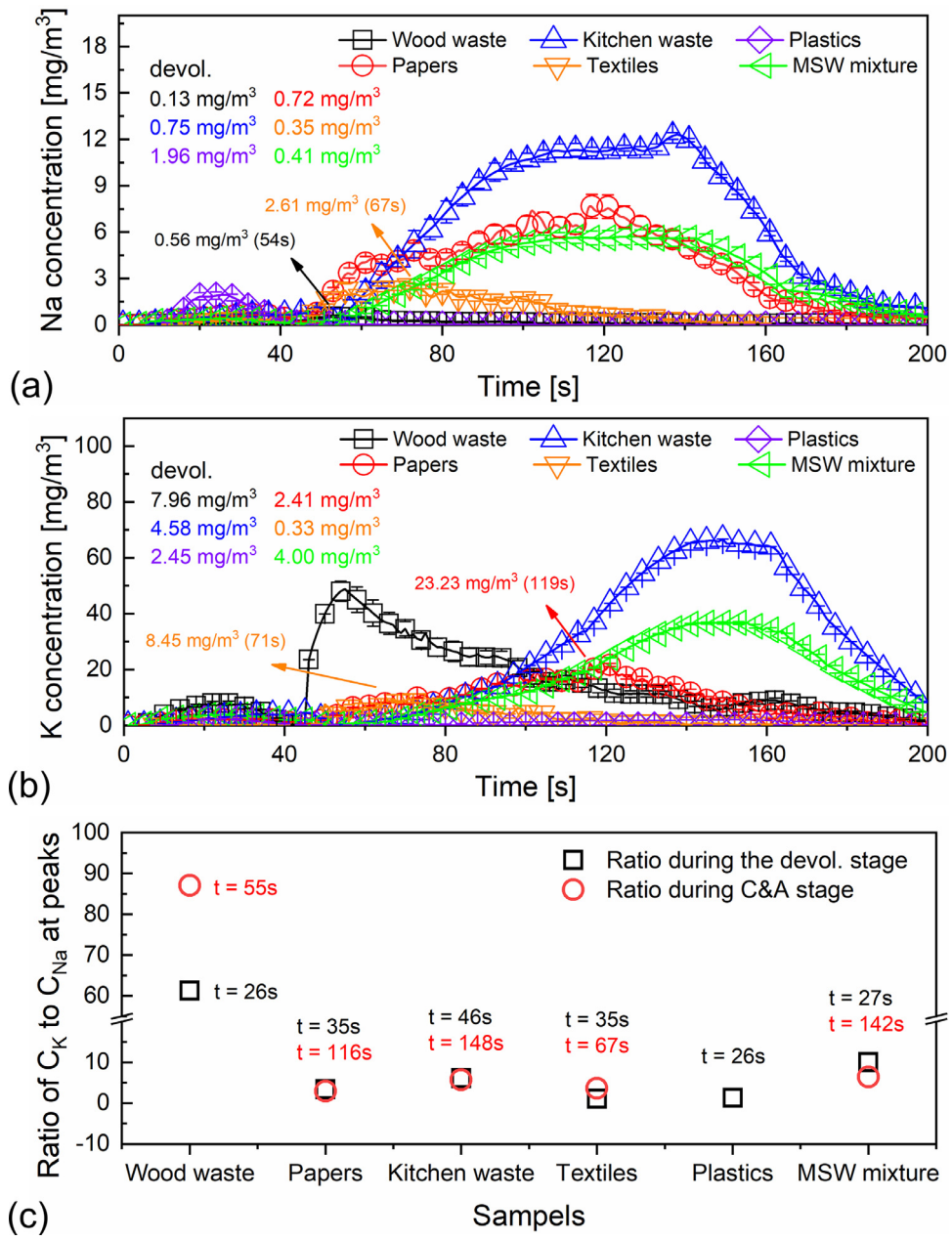

Fig. 6. Temporal release profiles of Na and K for the mixed waste fractions.

from the thermal radiation of the solid phase substances especially soot distributed in the flame. As reported in many studies [35,36], soot formation started with the small radicals produced during the fuel decomposition at the early stage of combustion. This led to the formation of larger radicals and polycyclic aromatic hydrocarbons (PAH) species widely accepted as precursors to soot formation. Generally, plastic materials generate more PAHs than biomass [37]. In addition, the presence of lignin with aromatic structures in biomass, compared to paper with very little lignin, contributes to an increase in soot yield by accelerating the formation rate of soot precursors [35]. Previous work [24] also found that flame-formed soot from burning wood showed smaller particle size and more ordered nanostructure than the soot generated from burning plastics, such as polyvinyl chloride, which, in turn, showed a higher oxidation tendency. It revealed that the chemical compositions of solid fuels could play an essential role in the physicochemical and radiative properties of soot particles in flames. Hence, although paper had a relatively high share of volatiles, it showed a small flame emissivity due to the lower soot volume fraction in the flame compared to other wastes. From another respective, high concentrations of soot particles for the plastic materials instead decreased the combustion efficiency for that the partial fuels were converted into soot rather than useful energy.

In addition, exciting work on the discrimination between different types of fuels by combining the FES method and a mathematical model has been proven feasible with high prediction accuracy [38]. The flame emission spectra from different waste fractions may also feature certain specificities; for example, plastic (textiles) exhibits a larger sooty spectrum than biomass species, despite the lack of deeper analysis.

3.3.2. Release behaviors of atomic sodium and potassium

Figure 6 provided the temporal release profiles of atomic alkali metals from the mixed fractions. All the samples, except plastics

which only showed one peak release shape, exhibited a typical bimodal peak shape, consistent with the observation in Section 3.2. It also indicated that Na and K featured identical trends in the release profiles despite the waste types.

To be specific, for example, the first peaks of the Na and K release concentrations from burning wood waste were measured to be 0.13 and 7.96 mg/m^3, respectively, while the second peaks were 0.56 and 48.76 mg/m^3, respectively. As discussed in the last section, the obtained peak concentrations were close to the values obtained from single wood-based materials. Similarly, paper and plastics also showed similar peak release concentrations for singe wastes with similar compositions. Because the measurement data at the second release peak were visible with much larger intensity than at the first peak, we compared the differences in the release patterns in the charring stage between the samples. In general, kitchen waste featured the highest peak concentration of 71.06 mg/m^3 among the samples, nearly 1.5 times that of wood waste. In contrast, the MSW mixture attained a medium value of 36.70 mg/m^3, whereas plastics (textiles) exhibited the lowest release peaks among the samples. Although wood waste and paper both belong to biomass, the higher K release concentration displayed by wood waste may be explained by the differences in the initial alkali content and chemical reactions during combustion: (i) A much higher fraction of potassium content in wood waste, as shown in Table 1, theoretically enables the release of more potassium than paper. (ii) The high total amounts of SiO_2 and Al_2O_3 in the paper (71%) (see Table S1) facilitate the chemical reactions of silicates (aluminosilicates) with potassium to form insoluble compounds before reaching the ash stage [39]. (iii) Potassium is increasingly released from burning wood waste because of the preferred reactions of silica with calcium rather than alkali metals.

The related chemical reactions and transformation mechanisms are much more complex [40] and are strongly affected by the fuel nature and experimental conditions. Textiles with relatively high potassium content exhibited the lowest release concentration of 8.45 mg/m^3. The most likely reason was that the high proportion of potassium in textiles was increasingly captured within the molten ash of glassy silicates.

The highest Na release was 12.21 mg/m^3 for the kitchen waste, which contained a high proportion of Na, while the lowest was only 0.56 mg/m^3 for wood waste. Overall, the release concentrations of Na were much lower than those of K, where the initial contents between them may be the key influencing factor. Beside, the K is more likely to be released than the Na for that K_2O owns a lower liquid/vapor distribution coefficient (0.5) compared to Na_2O (0.6) [41]. Another reason may be that the excited atoms decreased more for Na than for K because of the higher energy level of the excited state of Na when the temperature decreased [27]. Notably, the Na release distribution was similar for the MSW mixture and paper, with the maximum release concentrations second only to kitchen waste. It has been reported elsewhere [42] that paper is very reactive towards oxygen only after plastics among the common MSW materials. The additives in paper ash, such as kaolin and calcium carbonate, could significantly increase the reaction surface area by acting as catalysts or making the char more porous, which in turn promotes the release of Na and K in the early char stage, even though the additives may also transfer alkalis to the ash [9,16,43]. Figure 6c shows the relative ratio of Na and K concentrations at the two peaks. Independent of the fuel type, potassium exhibited a higher release level than sodium, especially for wood waste. The ratio values reached over 60 and 85 at the devolatilization and char stages, respectively.

3.3.3. Surface temperature and mass variation of waste pellets

Figure 7 provided the output data of the pellet-surface temperature recorded online by a K-type thermocouple. The pellet-surface

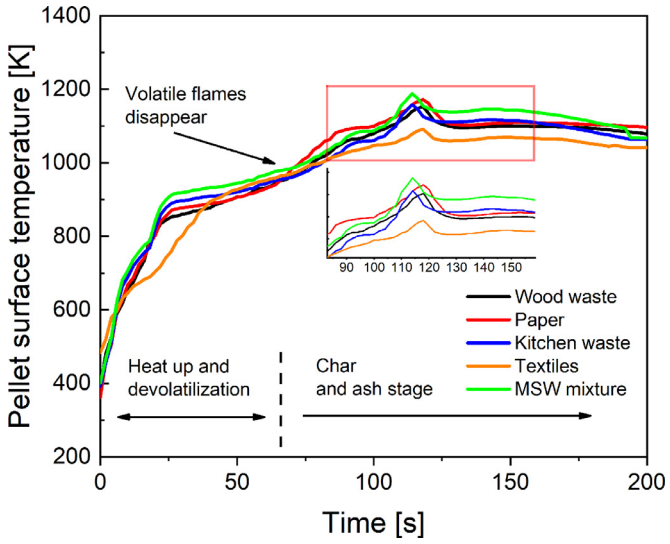

Fig. 7. Variation of the surface temperature of the mixed waste pellets during combustion.

temperature was critical to fuel pyrolysis and combustion rates by determining the heat flux generated to the particle center. Furthermore, the evolution in the pellet temperature could also represent the series of combustion phenomena. Plastic was excluded herein due to the absence of the char stage. As observed, from the moment at which the pellet was sent into the chamber, the pellet surface was rapidly heated up in the devolatilization stage due to the high-temperature co-flow and the thermal radiation from volatile flames; then, the surface temperature continued to increase with maxima at the char oxidation stage attributed to the thermal effect of char oxidation on the pellets; after that the temperature gradually decreased towards the equilibrium temperature in the late combustion stage with the consumption of char, where the inhibition of the ash layer on the char reactions was nonnegligible. A continuous increase in the pellet-surface temperature caused the reactions of the active and more exposed structures with oxygen. Hence, more alkalis were released in the char stage owing to the increased diffusion and oxidative reaction rates on the pellet surface that could enhance the bond breaking of most organic alkalis [40]. The identical results were also obtained by LIBS experiments [44]. It should be noted that the disappearance of volatile flames slowed down the increase rate in the temperature, which may explain for the gap between the two release peaks.

Figure 8 showed the temporal variation of the pellet mass during the combustion. The release concentrations of atomic alkali metals from the devolatilization stage to ash stage were integrated and normalized for semi-quantitative comparison, as shown in Fig. 8g. A sizeable mass reduction was seen in the devolatilization stage, at which most of the volatiles were released and then burnt out. Figure 8g suggested that the ratios of Na and K released at this stage mainly varied between 1 and 10% for the single/mixed waste fractions, which was very similar to the results conducted on raw biomass [16]. Additionally, although the mass loss rate was much lower in the char & ash stages compared to that in the devolatilization stage, most of the alkalis were released at this stage most likely due to the high pellet temperatures. It further revealed that the performance of alkali release was more dependent on the pellet-surface temperature, and less on the mass variation of the pellets during combustion.

The quality of the relationships between the peak release concentrations of Na and K detected by FES and the total content of those in the wastes was further explored, as shown in Fig. 9. There

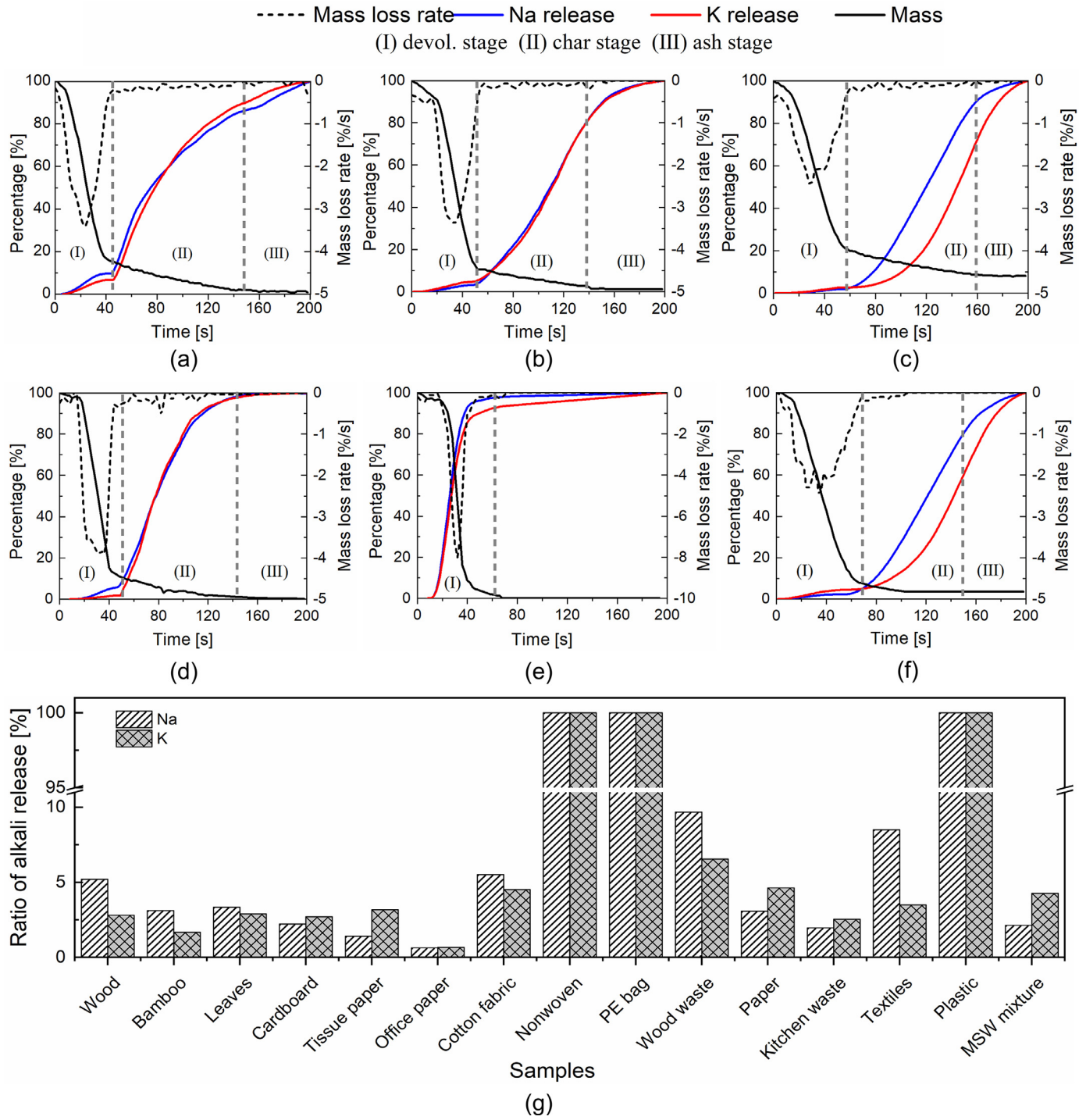

Fig. 8. Temporal changes of pellet mass and alkali release (normalized cumulative value) as a function of combustion time: Wood waste (a); Paper (b); Kitchen waste (c); Textiles (d); Plastics (e); MSW mixture (f); Ratios of alkali release in the devolatilization stage for all the wastes (g).

was a clear trend identifiable (with a regression function R^2 values of 0.75 and 0.90 for Na and K, respectively, in the char stage), which revealed that the peak release concentration occurring during char oxidation increased almost linearly with the initial concentration of alkalis in the pellets. This was in line with the fact that the established alkali release governed by the diffusion mechanism was proportional to the concentration gradient of the alkalis at the surface of the particle [16]. In contrast, in the volatile combustion stage, the peak Na/K concentrations were not related to the initial alkali content.

3.3.4. Transformation processes of alkali metals

The possible transformation routes of alkalis into the gas phase from waste burning are discussed [9,16,32,40], as shown in Fig. 10. Paper and wood waste essentially belong to biomass or biomass-based products. During volatile combustion, most gaseous alkalis likely originate from the evaporation and thermal decomposition of inorganic alkalis in the fuels. At this stage, some of the organic compounds (char-M) also decomposed to release atomic alkalis. For Cl-rich biomass, alkali metals are likely released in the form of KCl or NaCl during the devolatilization stage [45]. In the pres-

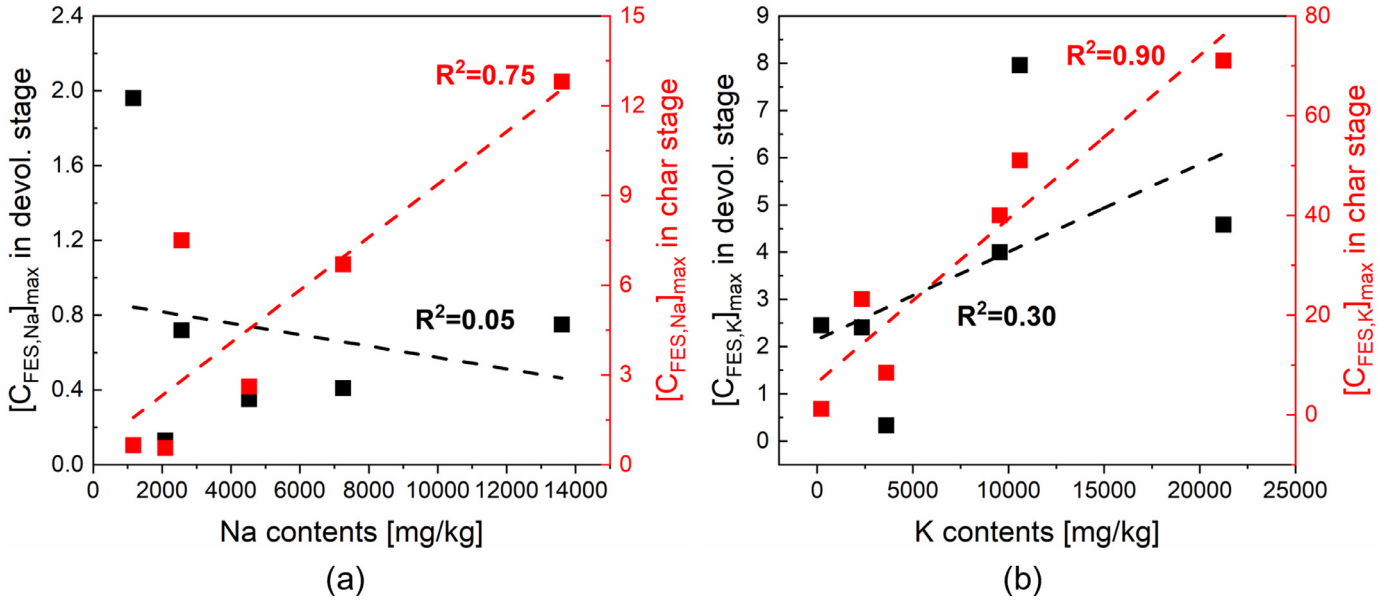

Fig. 9. Relationships between initial alkali contents in wastes with peak Na release concentrations (a) and peak K release concentrations (b).

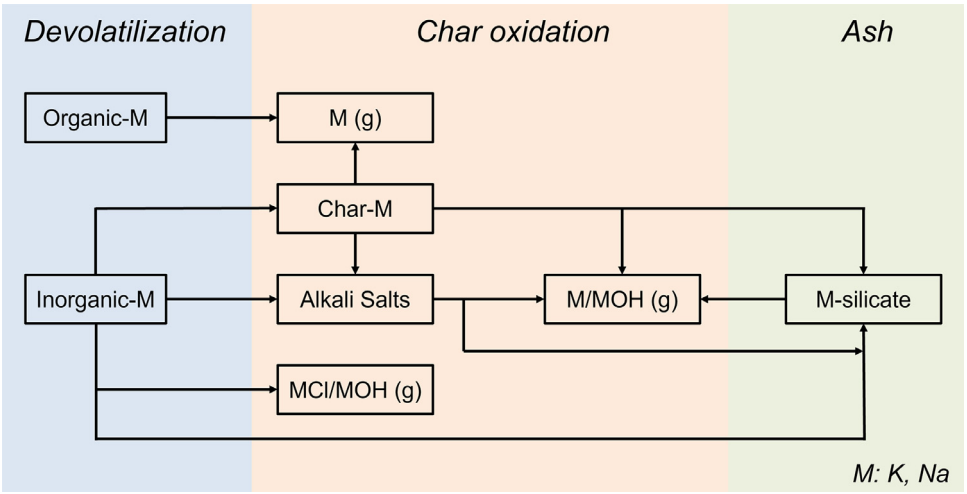

Fig. 10. Possible transformation routes of K and Na during waste combustion.

ence of moisture, alkalis can also take the form of alkali hydroxides (KOH or NaOH) and then evaporate physically from the burning pellets. However, Cl is quickly released into the gas phase as HCl, as reported by Zhang et al. [32], which indicates that the release of alkali hydroxide may be the dominant route during devolatilization. Residual Na and K mainly remained as char-alkali/char-O-alkali or mineral compounds. Accordingly, atomic alkalis would come from char-alkalis, carbonate, and sulfate through char oxidation and decomposition. Note that alkali metals can be transferred into ash in both the devolatilization and char stages. In the ash stage, although subtle, the ash can continuously react with vaporized water to further liberate gaseous KOH and NaOH [9]. In the real situation inside the furnace, as the mixed solid waste with a large amount of moisture at the bottom is exposed for more time to the high-temperature environment, the ratio of alkalis released in the ash stage may be larger.

For plastic-containing materials, such as plastics, since most of the alkali contents and pellet mass were consumed in the volatile combustion stage, they therefore featured relatively higher Na and K release concentrations than other biomass samples at this stage. Interestingly, the plastic content could melt when heated, forming a coating around the pellet surface. The melted plastic may inhibit the release of water-soluble alkalis; for example, the MSW mixture exhibited lower K release concentrations than wood waste, despite the similar K contents in Table 1. This is because some volatiles released from fuel pyrolysis and decomposition may be trapped inside the molten layer, which leads to the formation of secondary char via interactions between the volatiles and residual char/other volatile species [46].

4. Conclusions

This work firstly studied the release characteristics of sodium and potassium from burning multiple MSW fractions using calibrated flame emission spectroscopy (FES). The FES measurements were performed above a flat flame burner at a controled environmental temperature of 1073 K. The main conclusions are as follows:

The FES system was calibrated prior to the experiments in order to determine the actual alkali concentration in the flame. The calibration equation indicated that the alkali concentrations at the measuring point were dependent on the received FES spectral line

intensity of Na and K and the combustion temperature at the measuring point. The release of alkali metals occurred throughout the combustion process, and a three-stage releasing behavior, including devolatilization, char, and ash stages, can be distinguished for most wastes. It was also found that the concentrations of Na and K increased and then declined along the axial direction of the volatile flames. In contrast, the concentrations decreased monotonically to zero with increasing radial distance.

Specifically, kitchen waste featured the highest release concentrations of both Na (12.21 mg/m^3) and K (71.06 mg/m^3), owing to the highest initial alkali content among these samples. A large portion of the alkalis was released during the overlap combustion of volatiles and char as plastic (textiles) have shallow ash content. Beside, paper and wood waste possessed the second-largest amounts of Na and K, respectively, only second to kitchen waste. It also revealed that the initial alkali content served as the vital factor positively influencing the release characteristics, where the peak release concentration in the char stage increased almost linearly with the initial concentration of alkalis in the pellets. In addition to the fuel properties, the combustion characteristics of the pellets also took a vital role in the release characteristics of Na and K. The thermogravimetric profiles indicated that most of the pellet mass was burned out in the devolatilization stage; however, less than 10% of the alkali content was released at this stage. In contrast, the surface-pellet temperature was more important. The high pellet temperature contributed to an increase in the diffusion and reaction rates in the char stage, which, in turn, contributed to alkali release.

The transformation processes of alkali metals during the combustion of different wastes were discussed. For biomass-based materials and kitchen waste, the alkalis are released through pyrolysis and evaporation in the volatile combustion stage and decomposition and evaporation in the char and ash stages. However, for plastics (textiles), large amounts of alkali species are liberated during devolatilization because of the very high share of volatile matter. In addition, the results revealed that paper and wood waste were considered potential sources of Na and K release, respectively, once kitchen waste was wholly separated due to garbage classification in China.

Declaration of Competing Interest

The authors declare that they have no known competing financial interests or personal relationships that could have appeared to influence the work reported in this paper.

The authors declare the following financial interests/personal relationships which may be considered as potential competing interests:

Acknowledgments

This work is funded by the National Key Research and Development Program of China (2018YFC1901304) and Alibaba-Zhejiang University Joint Research Institute of Frontier Technologies.

Supplementary materials

Supplementary material associated with this article can be found, in the online version, at doi:10.1016/j.combustflame.2022.112233.

References

[1] Y. Ding, J. Zhao, J.W. Liu, A review of China's municipal solid waste (MSW) and comparison with international regions: management and technologies in treatment and resource utilization, J. Clean. Prod. 293 (2021) 126144.
[2] J.W. Lu, Y.S. Xie, B. Xu, From NIMBY to BIMBY: an evaluation of aesthetic appearance and social sustainability of MSW incineration plants in China, Waste Manag. 95 (2019) 325–333.
[3] J. Zhao, B. Li, X.L. Wei, Y.F. Zhang, T. Li, Slagging characteristics caused by alkali and alkaline earth metals during municipal solid waste and sewage sludge co-incineration, Energy 202 (2020) 117773.
[4] P. Viklund, A. Hjörnhede, P. Henderson, A. Stålenheim, R. Pettersson, Corrosion of superheater materials in a waste-to-energy plant, Fuel Process. Technol. 105 (2013) 106–112.
[5] S.V. Vassilev, C.G. Vassileva, Methods for characterization of composition of fly ashes from coal-fired power stations: a critical overview, Energy Fuels 19 (2005) 1084–1098.
[6] J. Zhang, C.L. Han, Z. Yan, K.L. Liu, Y.Q. Xu, C.D. Sheng, W.P. Pan, The varying characterization of alkali metals (Na, K) from coal during the initial stage of coal combustion, Energy Fuels 15 (2001) 786–793.
[7] L.J. Hsu, Z.T. Alwahabi, G.J. Nathan, Y. Li, Z.S. Li, M. Aldén, Sodium and potassium released from burning particles of brown coal and pine wood in a laminar premixed methane flame using quantitative laser-induced breakdown spectroscopy, Appl. Spectrosc. 65 (2011) 684–691.
[8] Y.Z. Liu, Y. He, Z.H. Wang, K.D. Wan, J. Xia, J.Z. Liu, K.F. Cen, Multi-point LIBS measurement and kinetics modeling of sodium release from a burning Zhundong coal particle, Combust. Flame 189 (2018) 77–86.
[9] Y.Z. Liu, Z.H. Wang, J. Xia, L. Vervisch, K.D. Wan, Y. He, R. Whiddon, H. Bahai, K.F. Cen, Measurement and kinetics of elemental and atomic potassium release from a burning biomass pellet, Proc. Combust. Inst. 37 (2019) 2681–2688.
[10] K. Kohse-Höinghaus, R.S. Barlow, M. Aldén, Combustion at the focus : laser diagnostics and control, Proc. Combust. Inst. 30 (2005) 89–123.
[11] J. Ballester, T. García-Armingol, Diagnostic techniques for the monitoring and control of practical flames, Prog. Energy Combust. Sci. 36 (2010) 375–411.
[12] J.M. Jones, L.I. Darvell, T.G. Bridgeman, An investigation of the thermal and catalytic behaviour of potassium in biomass combustion, Proc. Combust. Inst. 31 (2017) 1955–1963.
[13] R. Navakas, A. Saliamonas, N. Striūgas, A. Džiugys, R. Paulauskas, K. Zakarauskas, Effect of producer gas addition and air excess ratio on natural gas flame luminescence, Fuel 217 (2018) 478–489.
[14] F.M. Quintino, T.P. Trindade, E.C. Fernandes, Biogas combustion: chemiluminescence fingerprint, Fuel 231 (2018) 328–340.
[15] R. Paulauskas, N. Striugas, M. Sadeckas, P. Sommersacher, S. Retschitzegger, N. Lienzl, Online determination of potassium and sodiumrelease behaviour during single particle biomass combustion by FES and ICP-MS, Sci. Total Environ. 746 (2020) 141162.
[16] P.E. Mason, L.I. Darvell, J.M. Jones, A. Williams, Observations on the release of gas-phase potassium during the combustion of single particles of biomass, Fuel 182 (2016) 110–117.
[17] P.E. Mason, J.M. Jones, L.I. Darvell, A. Williams, Gas phase potassium release from a single particle of biomass during high temperature combustion, Proc. Combust. Inst. 36 (2017) 2207–2215.
[18] Z.L. He, C. Lou, J.T. Fu, M. Lim, Experimental investigation on temporal release of potassium from biomass pellet combustion by flame emission spectroscopy, Fuel 253 (2019) 1378–1384.
[19] K.Y. Li, W.J. Yan, X.L. Huang, L.B. Yu, Y.M. Chen, C. Lou, *In-situ* measurement of temperature and potassium concentration during the combustion of biomass pellets based on the emission spectrum, Fuel 289 (2021) 119863.
[20] K.Y. Li, W.J. Yan, Simultaneous determination of Na concentration and temperature during Zhundong coal combustion using the radiation spectrum, Energy Fuels 35 (2021) 3348–3359.
[21] C. Lou, Y. Pu, Y.G. Zhao, An *in-situ* method for time-resolved sodium release behaviour during coal combustion and its application in industrial coal-fired boilers, Proc. Combust. Inst. 38 (2021) 4199–4206.
[22] X.L. Li, C.X. Han, Online dynamic prediction of potassium concentration in biomass fuels through flame spectroscopic analysis and recurrent neural network modelling, Fuel 304 (2021) 121376.
[23] X.H. He, C. Lou, Y. Qiao, M. Lim, *In-situ* measurement of temperature and alkali metal concentration in municipal solid waste incinerators using flame emission spectroscopy, Waste Manag. (2020) 486–491.
[24] J.J. He, Q.X. Hu, M.N. Jiang, Q.X. Huang, Nanostructure and reactivity of soot particles from open burning of household solid waste, Chemosphere 269 (2021) 129395.
[25] H. Zhou, A.H. Meng, Y.Q. Long, Q.H. Li, Y.G. Zhang, An overview of characteristics of municipal solid waste fuel in China: physical, chemical composition and heating value, Renew. Sustain. Energy Rev. 36 (2014) 107–121.
[26] Q.Y. Chen, Y.S. Wang, J. Li, Z.H. Liu, Experimental investigation of pressurized combustion characteristics of a single coal particle in O_2/N_2 and O_2/CO_2 environments, Energy Fuels 33 (2019) 12781–12790.
[27] S. Zheng, Y. Yang, X.Y. Li, H.W. Liu, W.J. Yan, R. Sui, Q. Lu, Temperature and emissivity measurements from combustion of pine wood, rice husk and fire wood using flame emission spectrum, Fuel Process. Technol. 204 (2020) 106423.
[28] W.J. Yan, K.Y. Li, X.L. Huang, L.B. Yu, C. Lou, Y.M. Chen, Online measurement of the flame temperature and emissivity during biomass volatile combustion using spectral thermometry and image thermometry, Energy Fuels 34 (2020) 907–919.
[29] D.K. Zhang, T.F. Wall, P.C. Hills, The ignition of single pulverized coal particles: minimum laser power required, Fuel 73 (1994) 647–655.
[30] W.R. Lea, Plastic incineration versus recycling: a comparison of energy and landfill cost savings, J. Hazard. Mater. 47 (1996) 295–302.

[31] P. Eyk, P.J. Ashman, Z.T. Alwahabi, G.J. Nathan, The release of water-bound and organic sodium from Loy Yang coal during the combustion of single particles in a flat flame, Combust. Flame 158 (2011) 1181–1192.
[32] Z.H. Zhang, Q. Song, Z.T. Alwahabi, Q. Yao, G.J. Nathan, Temporal release of potassium from pinewood particles during combustion, Combust. Flame 162 (2015) 496–505.
[33] Y.Z. Liu, K.D. Wang, Experimental study of potassium release during biomass-pellet combustion and its interaction with inhibitive additives, Fuel 260 (2020) 116346.
[34] R. Paulauskas, N. Striugas, K. Zakarauskas, A. Dziugys, L. Vorotinskiene, Investigation of regularities of pelletized biomass thermal deformations during pyrolysis, Therm. Sci. 22 (2018).
[35] C.X. Sun, J. Martin, A.L. Boehman, Nanostructure and reactivity of soot produced from a turbodiesel engine using post injection, Proc. Combust. Inst. 37 (2019) 1169–1176.
[36] A.D. Sediako, C. Soong, J.Y. Howe, Real-time observation of soot aggregate oxidation in an environmental transmission electron microscope, Proc. Combust. Inst. 36 (2017) 841–851.
[37] H. Zhou, et al., Aromatic hydrocarbons (PAH) formation from the pyrolysis of different municipal solid waste fractions, Waste Manag. 36 (2015) 136–146.
[38] J.M. De Paulo, J.E.M. Barros, P.J.S. Barbeira, A pls regression model using flame spectroscopy emission for determination of octane numbers in gasoline, Fuel 176 (2016) 216–221.
[39] D.S. Clery, P.E. Mason, C.M. Rayer, J.M. Jones, The effects of an additive on the release of potassium in biomass combustion, Fuel 214 (2018) 647–655.
[40] W.H. Cao, J. Li, L.T. Lin, X.L. Zhang, Release of potassium in association with structural evolution during biomass combustion, Fuel 287 (2021) 119524.
[41] D. Poole, V. Sharifi, J. Swithenbank, B. Argent, D. Ardelt, On-line detection of metal pollutant spikes in MSW incinerator flue gases prior to clean-up, Waste Manag. 27 (2007) 519–532.
[42] M. Nikku, A. Deb, E. Sermyaina, L. Puro, Reactivity characterization of municipal solid waste and biomass, Fuel 254 (2018) 115690.
[43] A. Hosan, S. Haque, F. Shaikh, Compressive behaviour of sodium and potassium activators synthetized fly ash geopolymer at elevated temperatures: a comparative study, J. Build. Eng. 8 (2016) 123–130.
[44] C. Oris, Z.Y. Luo, E.G. Eddings, C.J. Yu, Determination of alkali release during oxyfuel co-combustion of biomass and coal using laser-induced breakdown spectroscopy, Fuel 289 (2021) 119658.
[45] X. Li, F. He, X. Su, F. Behrendt, Z. Gao, H. Wang, Evaporation rate of potassium chloride in combustion of herbaceous biomass and its calculation, Fuel 257 (2019) 116021.
[46] Y.P. Rago, F.X. Collard, J.F. Gorgens, D. Surroop, R. Mohee, Torrefaction of biomass and plastic from municipal solid waste streams and their blends: evaluation of interactive effects, Fuel 277 (2020) 118089.